


Article

Simulations of Deformation Failure Process and Refinement of Reinforcement Scheme in the Dabenliu Quarry Slope Using Discontinuous Deformation Analysis

Wei-Hua Hou¹, Feng Xiong^{2,*}  and Qi-Hua Zhang¹

¹ Badong National Observation and Research Station of Geohazards, China University of Geosciences, Wuhan 430074, China; houweihua@cug.edu.cn (W.-H.H.); zhangqh@cug.edu.cn (Q.-H.Z.)

² Faculty of Engineering, China University of Geosciences, Wuhan 430074, China

* Correspondence: fengxiong@cug.edu.cn; Tel.: +86-67883124

Abstract: For this study, the geological engineering features and possible failure modes of the Dabenliu quarry slope in the Jinping-I Hydropower Station were qualitatively analyzed before a method for setting viscous boundary and an algorithm for modeling pre-stressed cables were embedded into a DDA (Discontinuous Deformation Analysis) computer code to analyze the deformation of the slope under seismic loading. Our simulation results revealed that the middle and upper parts of the slope slipped along the bedding joints (interlayer shear zones) and that the lower part buckled and collapsed after the slope was excavated. This is a typical slipping–buckling failure mode characterized by upper-slipping followed by lower-buckling. Based on the distribution of the simulated internal force of the anchor cables, the reinforcement scheme was adjusted by strengthening the support for the middle and lower parts of the slope, whereas the length and pre-stress of the anchor cables were reduced for the upper part of the slope. The adjusted reinforcement scheme can ensure the stability of the slope under the action of a magnitude 7 earthquake, and the slope may lose stability with no evident collapse under the action of a magnitude 8 earthquake. Finally, the simulation results were verified via a comparison with the monitoring data regarding the slope.



Citation: Hou, W.-H.; Xiong, F.; Zhang, Q.-H. Simulations of Deformation Failure Process and Refinement of Reinforcement Scheme in the Dabenliu Quarry Slope Using Discontinuous Deformation Analysis. *Appl. Sci.* **2023**, *13*, 11010. <https://doi.org/10.3390/app131911010>

Academic Editors: Qingxiang Meng, Tingting Luo, Susheng Wang and Peng Wu

Received: 1 September 2023

Revised: 28 September 2023

Accepted: 4 October 2023

Published: 6 October 2023



Copyright: © 2023 by the authors. Licensee MDPI, Basel, Switzerland. This article is an open access article distributed under the terms and conditions of the Creative Commons Attribution (CC BY) license (<https://creativecommons.org/licenses/by/4.0/>).

Keywords: discontinuous deformation analysis (DDA); slope stability analysis; deformation failure process; seismic loading; anchor reinforcement

1. Introduction

The Jinping-I Hydropower Station is located in the Yalongjiang river of Western China, and it has an installed capacity of 3600 MW. The Dabenliu quarry slope is located in the downstream of the dam and the left bank of the Yalongjiang river. The max excavation height of the quarry slope is 468 m, and the excavation slope ratio is fairly large, forming a precipitous man-made high-steep slope, as shown in Figures 1 and 2. In order to meet the requirements of material consumption for dam construction, the slope excavation speed is fast, and the phenomena of rock deformation, cracking and collapse frequently occur during excavation. As one of the highest bedding steep rock slopes in China, more attention is being paid to the stability and safety of quarry slopes by the government, designers, and construction contractors during the construction period.

The Dabenliu slope at the dam site is characterized by a steep geometry and complex geological conditions. Figure 2 shows a plan view of this slope, along with a plan of the topography and excavation of the quarry slope. The geological profile (1₁-1₁) of the slope is shown in Figure 3. The slope rock masses are composed of marble (T_{2-3Z}²), slate, and stratified metasandstone (T_{2-3Z}³), which were formed in the Zagunao formation in the Middle and Upper Trias. The overall strike of the strata in the area is in the range of 350° to 30°, the dip direction is about SE, and the dip angle is about 64° to 72°. Under the influence of tectonic action, the local strata are deflected and even bended, the strike changes to about

40° to 56°, and the dip becomes steeper, increasing from 80° to 85°. There are thin and soft layers (clayey interbeds) embedded in the hard strata, which have undergone a series of interlayer shearing and argillization processes through the action of multi-phase tectonic stress, finally forming a lot of interlayer shear zones. The interlayer shear zones are widely developed and are located at different depths beneath the subsurface of the slope, with a spacing of 4–7 m and a thickness of 0.5–5 cm, as shown in Figure 2. In addition, there are small faults and many groups of joints in the slope rock masses. Most of the small faults intersect with the slope at a large angle or even incline inward the slope, such as F12, F17, F18, and F113 (Figure 2). Moreover, four sets of joints exist in the rocks. The first set includes bedding joints with an orientation of N 60°–90° E. The other sets are oriented at N 270°–300° W, N 300°–330° W, and N 30°–60° E. In a word, it can be concluded that the geological conditions at the slope zone are extremely complex.

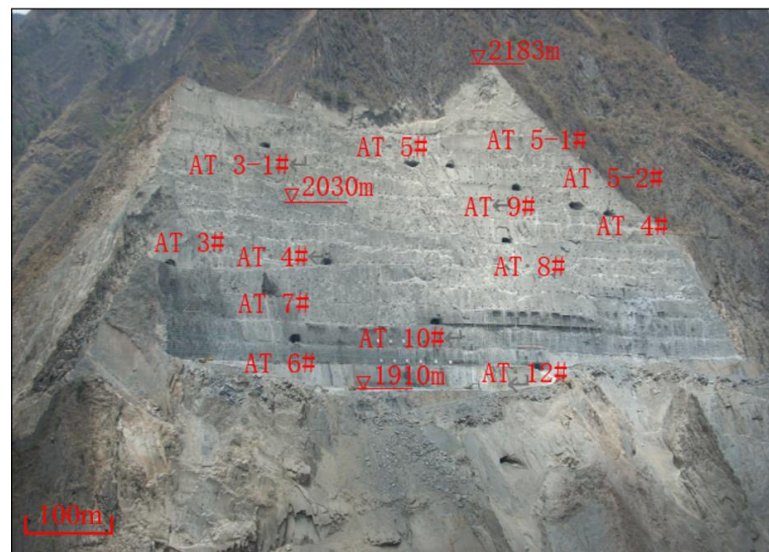


Figure 1. Quarry slope excavation. Legend: AT—Access tunnel.

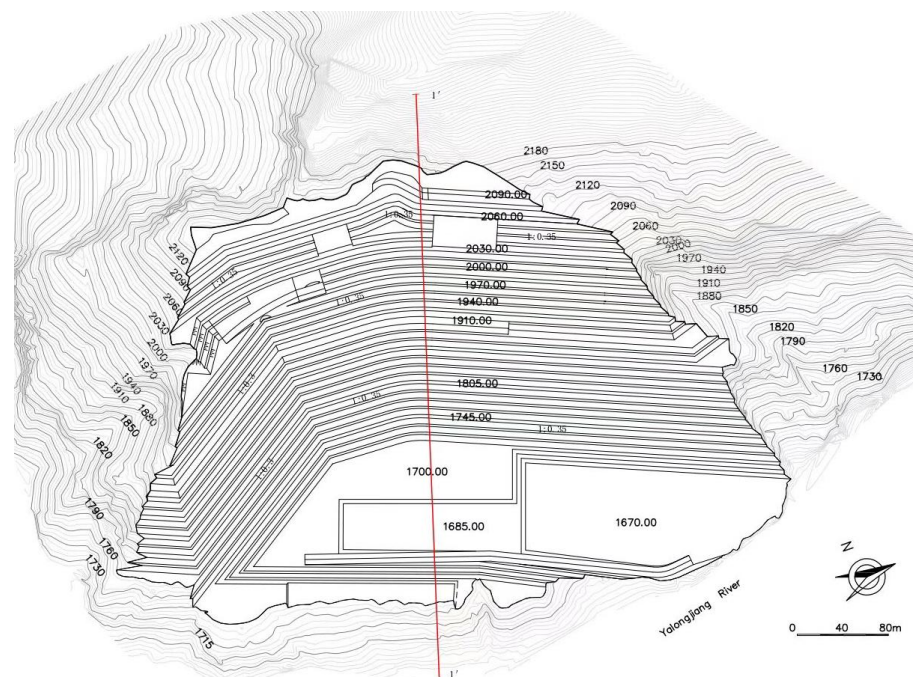


Figure 2. Plan of topography and excavation of the quarry slope.

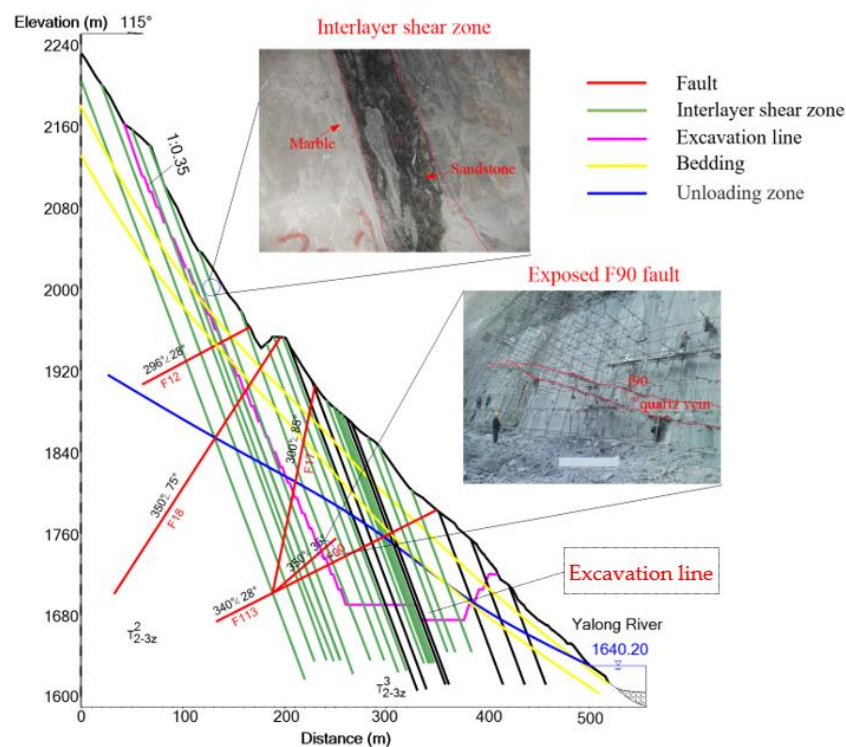


Figure 3. Geological cross section I1-I1 of the Dabenliu quarry slope.

The quarry slope can be divided into two main parts according to the change in the strike of the slope after excavation: the north–west front slope, and the south–west side slope. In the north–west front slope, which also constitutes the main part of the quarry slope, the strike of the strata is nearly parallel to the slope strike and steeply inclines outside the slope. However, the dip of the strata is larger than the slope angle (see Figure 2); hence, it seems that the strata are obliquely inserted into the ground, and the natural slope is stable as a whole. In the south–west side slope, the strata strike obliquely intersects with the slope strike, and the slope is more stable than the north–west front slope before excavation.

The DDA method is an excellent numerical method that can simulate large deformation problems in relation to slopes [1,2]. The slope of the quarry slope may undergo significant deformation. There has been in-depth research on DDA deformation simulation both domestically and internationally, as shown in Table 1. However, there are few reports on using DDA to simulate deformation under seismic loads [3–5].

Table 1. Literature review of DDA simulation.

Number	Source	Contribution
1	[6]	A cusp catastrophe model is proposed for a slip–buckling slope based on catastrophe theory, and the formulations of the necessary and sufficient conditions for instability of the slope are presented.
2	[7]	Qualitative assessment visually examining runtime behavior of simulations, semi-quantitative assessment comparing numerical results of simulations, and quantitative assessment wherein the numerical simulation results are evaluated in detail with respect to similar analytical, laboratory or field results. DDA performs more than adequately for engineering analysis.
3	[8]	Research has shown that, under seismic loads, the slope model mainly presents shear cracks and tension cracks that extend, connect, and develop step-type fractures; the slope experienced toppling and sliding failure. The study has theoretical and practical significance, it can provide guidance for seismic slope engineering.
4	[9]	To improve contact precision in the DDA, an augmented Lagrangian method, which can make use of advantages of both the Lagrangian multiplier method and the penalty method, is introduced.
5	[10]	Research has shown that discontinuous deformation analysis (DDA) is capable of modeling rockslides with substantial debris flow.

Table 1. *Cont.*

Number	Source	Contribution
6	[11]	Research shows the validation of two methods of wedge stability analysis, namely, block theory and three-dimensional discontinuous deformation analysis (3D DDA), using physical models and field case histories.
7	[12]	Simulations of real rockfall via discontinuous deformation analysis (DDA) are conducted. This novel technique properly considers the energy absorption ability of the slope based on vegetation conditions and the shape of rockfall and provides a new method for the assessment and preventive design of rockfall.
8	[13]	The DDA method clearly shows the process of rock block failure and profoundly reveals the difference in sliding mode (caused by using different stability evaluation methods).

2. Possible Failure Modes of the Slope

The Dabenliu quarry slope is a typical high-steep bedding slope. As discussed above, there are three kinds of discontinuities in the rock masses of the slope: interlayer shear zones (bedding joints), small faults, and cross joints. The layers themselves are relatively hard, with high persistence, whereas there are numerous interlayer shear zones with a small spacing compared with the height of the slope. It seems that the slope is composed of a series of thin slabs obliquely superimposed together.

After the slope is excavated, the dip of the strata is nearly equal with the angle of the excavated slope in the north–west front slope, as the excavation lines depict in Figure 3. However, the strata in the south–west side slope intersect obliquely with the slope strike. At the same time, there are a lot of small faults and cross joints within the rock strata. The failure of the slope may manifest in the following modes after excavation:

(1) Slipping–buckling failure. The north–west front slope is a dip slope, with the dip angle of strata being almost parallel to the slope gradient. Even though layers never daylight at the slope toe, the exceptional persistence and weakness of the interlayer shear zones allow for the buckling of layers. In the initial stage after excavation, the middle and upper parts of the slope strata may slip slowly along the bedding joints because the strata are so steep and the shear strength of the bedding joints is so weak to the point whereby it cannot resist the huge sliding force proceeding downslope. The slipping deformation may be very small since the bedding joints at the slope toe are not daylighted; however, a small deformation is enough to cut off the cohesion between layers. Then, the huge self-weight of the middle and upper layers may transfer to the lower part with a finite width, causing the lower part to gradually buckle. The buckling occurs more easily when triggered by an earthquake or when cross joints exist. Because the strata are hard, thin, and highly persistent with a lot of cross joints and small faults, the failure will manifest as block extrusion and collapse. These modes are shown in Figure 4. Its occurrence may cause a large-scale rock avalanche.

(2) Slipping along the interlayer. This failure mode happened in the south–west side of the slope on 29 June 2011. The crushed rock was composed of the thin–extremely thin slates located between the elevation of 1895 and 1930 m. The length of the crushed rock was about 3–5 m along the slope surface and 2–3 m in depth, and the volume was about 550 m³, as shown in Figure 5.

(3) Block failure. During slope excavation, unstable blocks can be formed under a certain number of unfavorable combinations of joints, interlayer shear zones, or small faults. This mode occurred in the south–west side of the slope on 5 July 2011. The crushed rock, located between the elevation of 1925 and 1985 m, was composed of the metamorphic quartz strata interlayered with the slates. Its morphology was akin to a tetrahedron block, and it had a volume of about 4100 m³, as shown in Figure 6. The small fault F2 along with some interlayer shear zones formed the cutting faces of the block.

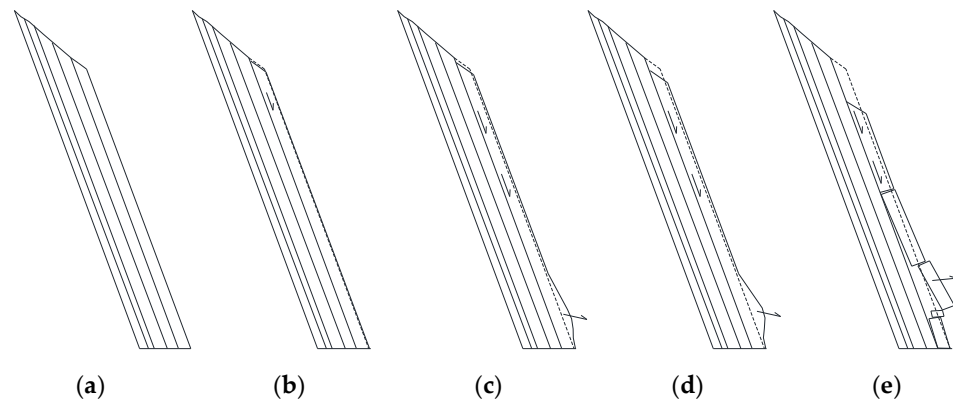


Figure 4. Schematic diagram of slipping–buckling failure mode: (a) the slope is composed of a series of thin strata with interlayer shear zones in it; (b) the outer strata begin to slip in the upper part; (c) the slipping develops to the middle and bottom parts, and the bottom parts begin to buckle and extrude outward due to the great weight of the middle and upper parts acting on the limit width of the lower parts; (d) these deformation failure phenomena accumulate, ultimately causing a (e) collapse.



Figure 5. Slipping along interlayer.

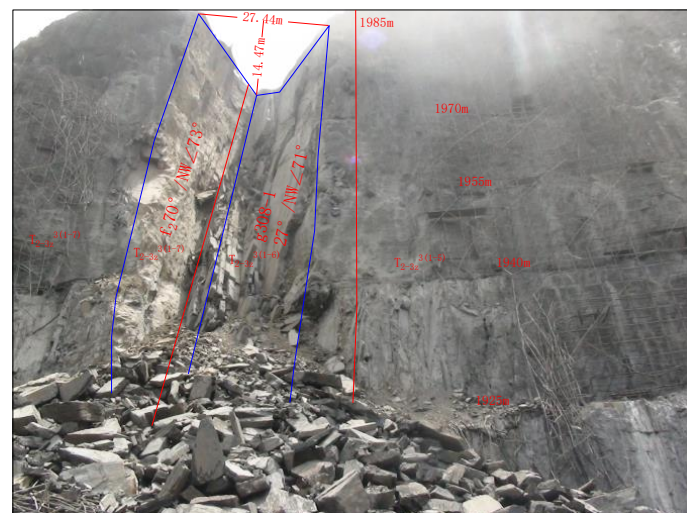


Figure 6. Block failure.

Hence, the possibility of rock failure, the above failure modes, and the deformation failure process, together with stability during excavation and long-term stability, are the key issues in slope excavation design. Through qualitative analyses and comprehensively considering the aspects of the geological characteristics of the three kinds of discontinuities, the features of the above three failure modes, and the possible scale of the failure strata, as well as the difference in the strike between the front and side slopes, one can ascertain that the slipping–bulking failure is more dangerous as it may cause strata failure from the top to the bottom of the slope [14–17]. At the same time, this mode concerns the analysis of the deformation failure process, and the relevant studies regarding this type of failure mode are much more limited compared with the other two kinds of failure modes.

Qin et al. [6] analyzed the mechanical mechanism of buckling failure. In their study, a cusp catastrophe model was developed based on catastrophe theory and the formulations of the necessary and sufficient conditions for the instability of the slope were presented. Tommasi et al. [18] analyzed the genetic mechanism of the buckling failure in a typical dip slope with a gentle gradient in the left flank of the Adige River valley south of Rovereto (North-Eastern Italy), as shown in Figure 7. In their study, this failure mode was back-analyzed using the Distinct Element Method (DEM) and Discontinuous Deformation Analysis (DDA). Seijmonsbergen et al. [19] explored the mass source of the sturzstroms originating from prehistoric landslides and rock avalanches that occurred at the end of a glacial retreat in Vorarlberg, Austria. They believed that the sturzstroms were produced by a three-hinge buckling failure that happened on the dip slopes due to alternating sandstone, marl, and conglomerate layers.

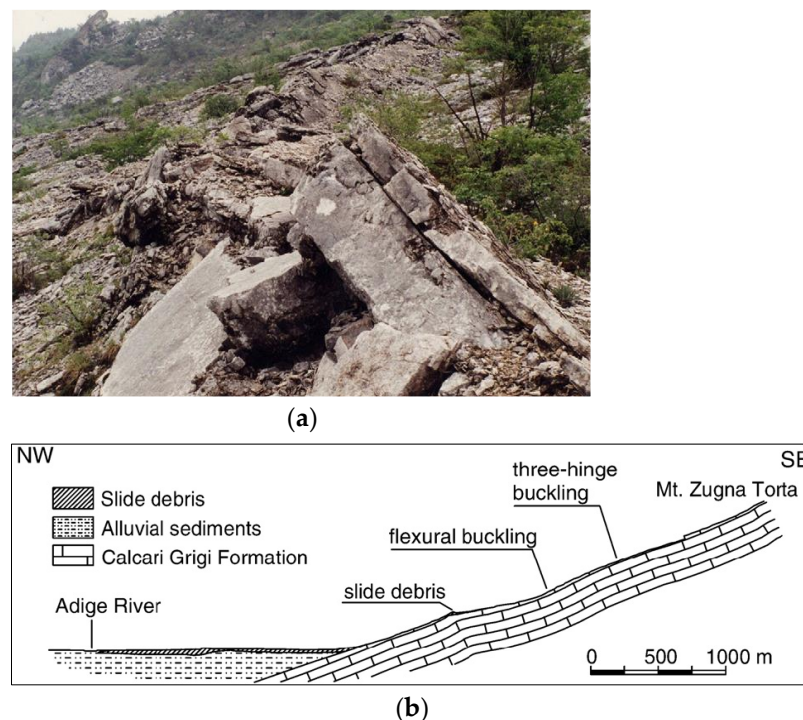


Figure 7. The buckling failure (from Tommasi et al., 2009). (a) Actual scene; (b) Pprofile of the left flank of the Adige Valley.

In contrast with the above work, this article studies the deformation failure processes of buckling failure triggered by excavation and earthquakes in the Dabenliu quarry slope. This slope and its strata are higher and steeper than most of those in the literature. The effect of the reinforcement scheme will also be evaluated and refined accordingly. Many discontinuity-based methods, including DDA, DEM, the combination of FEM and DDA [20], and the coupled DDA-SPH method [21], were used to simulate the deformation failure processes of geological materials. Considering the possible features of deformation failure

regarding the quarry slope under study, fragmentation may be not serious, and most of the blocks will likely remain intact; thus, we deemed it suitable to use the DDA method as an analysis tool for the present study. Discontinuous deformation analysis (DDA), which is of rigid mathematical and mechanical foundation, is capable of analyzing large displacement and failure processes in complicated block systems.

3. Some Relevant Simulation Technologies in DDA

Discontinuous deformation analysis (DDA) [22] is a numerical method for analyzing the discontinuous deformation of a block system. DDA constructs equilibrium equations for dynamic problems in an incremental form based on the principle of potential energy minimization. It introduces the real inertia force and uses a dynamic method to solve static (including quasi-static) and dynamic problems. For static problems, damping is adopted to absorb the kinetic energy of the block system in order to achieve a final static equilibrium state. Since it can simulate the actual mechanical process (the current static state of the block system is actually the result of a series of dynamic processes) of rock masses, the calculated results, including the contact forces between the blocks and the displacements, are of practical significance. Owing to the great advantages brought by the simulations of large deformation and discontinuous deformation in the DDA method, the blocks are allowed to move and deform as time progresses, and the mode of failure (if any) of the rock mass simulation model becomes apparent without the need to involve preliminary assumptions.

DDA meets three convergence conditions: convergence of the equilibrium equations, convergence of the open–close iterations for all contacts, and convergence of the maximum displacement for static computations [23]. In each computation step, it usually needs several open–close iterations to adjust the contact patterns of opening, closing, or sliding until the contact pattern at each contact position does not change. By applying or removing the rigid springs on the interfaces between blocks, the contact patterns satisfying non-entrance and non-tension between blocks are realized. Then, the computation proceeds to the next step. Thus, in each open–close iteration analysis of each time step, DDA must solve the global equilibrium equations. The open–close iteration ensures that the conditions of non-entrance and non-tension are strictly obeyed among the blocks. Hence, the theory is rigid and of high computation efficiency.

Ever since DDA was first proposed, it has received extensive attention and attracted considerable interest. Many studies on physical model testing and DDA verification [7,8,24–27], block contact problems [9,10,28], three-dimensional DDA methods [11,29–31], dynamic stability analysis [32–36], and engineering applications [12,13,37–40] have been carried out.

Even though DDA is a powerful analysis tool for the stability evaluation of rock engineering, it has not been as widely employed in practice compared to other popular numerical computation methods due to the relative difficulties with respect to its theoretic bases and the fact that it usually requires application technologies.

For this study, a method for viscous boundary setting for calculating the dynamic deformation of a slope under seismic loading and an algorithm for modeling a pre-stressed cable were embedded into the DDA computer code. The effect of the reinforcement for the slope under seismic loading was also simulated and discussed.

3.1. Viscous Boundary Setting

A viscous boundary condition was introduced into the DDA computer code by setting free dampers in the normal and tangential boundary of all blocks (Figure 8). The normal and tangential damping stresses, f_n and f_s , are as follows:

$$f_n = -\rho c_P v_n \quad (1)$$

$$f_s = -\rho c_S v_s \quad (2)$$

where ρ is the density of media; c_P and c_S are P -wave velocity and S -wave velocity, respectively; v_n and v_s are the normal and tangential components of velocity at the boundary. c_P and c_S can be obtained as follows:

$$c_P = \sqrt{\frac{E(1-\nu)}{\rho(1+\nu)(1-2\nu)}} \tag{3}$$

$$c_S = \sqrt{\frac{E}{2\rho(1+\nu)}} \tag{4}$$

where E and ν are the module and Poisson's ratio of media.

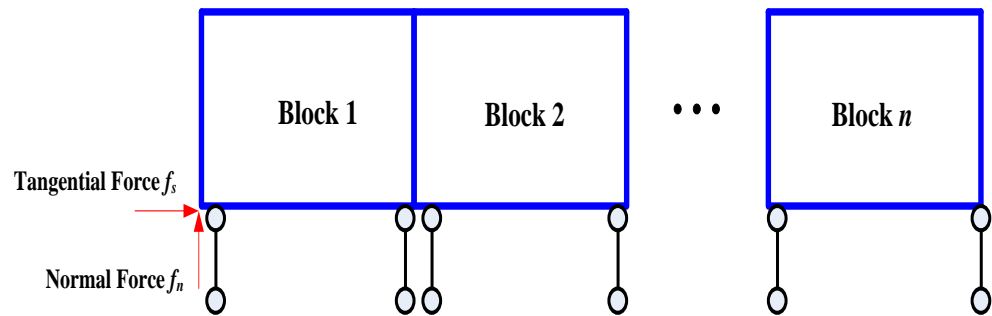


Figure 8. Viscous boundary in DDA.

3.2. Pre-Stressed Cable Numerical Realization in DDA

As shown in Figure 9, a pre-stressed cable connects block $i(x_i, y_i)$ and $j(x_j, y_j)$. The increase in cable length is as follows:

$$\begin{aligned} dl &= \frac{1}{l} [(x_1 - x_2)(u_1 - u_2) + (y_1 - y_2)(v_1 - v_2)] + \frac{f_0}{s} \\ &= (u_1 \ v_1) \begin{pmatrix} l_x \\ l_y \end{pmatrix} - (u_2 \ v_2) \begin{pmatrix} l_x \\ l_y \end{pmatrix} + \frac{f_0}{s} \\ &= D_i^T \begin{pmatrix} l_x \\ l_y \end{pmatrix} - D_j^T \begin{pmatrix} l_x \\ l_y \end{pmatrix} + \frac{f_0}{s} \end{aligned} \tag{5}$$

where D is the displacement vector in DDA; f_0 and s are the anchorage pre-stress and stiffness, respectively. The strain energy of cable is as follows:

$$\Pi = \frac{e_0}{2} \left(dl + \frac{f_0}{s} \right)^2 = D_i^T E_i E_i^T D_i - 2D_i^T E_i G_j^T G_j + D_j^T E_j E_j^T D_j \tag{6}$$

where $E_i = T_i^T(l_x, l_y)^T$ and $G_j = T_j^T(l_x, l_y)^T$. By taking the extreme value of Equation (6), six linear equations can be obtained; these equations were added into the global stiffness matrix of DDA, i.e.,

$$\left. \begin{aligned} sE_i^T E_i &\rightarrow K_{ii} \\ sG_j^T G_j &\rightarrow K_{jj} \\ -sE_i^T G_j &\rightarrow K_{ij} \\ -sG_j^T E_i &\rightarrow K_{ji} \\ -f_0 E_i &\rightarrow F_i \\ f_0 G_j &\rightarrow F_j \end{aligned} \right\} \tag{7}$$

where K is the global stiffness matrix and F is the loading vector.

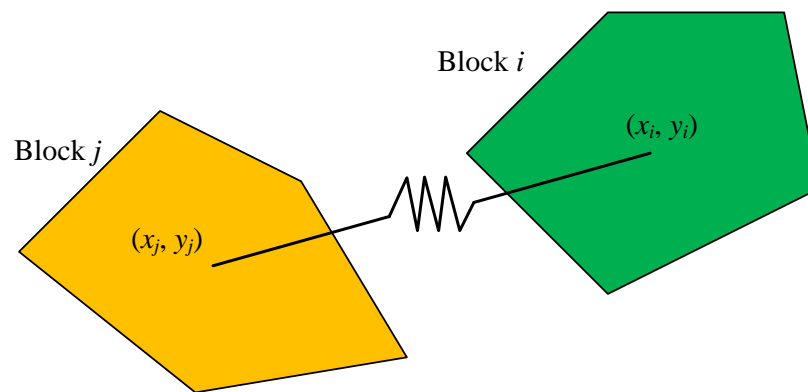


Figure 9. Pre-stressed cable connects blocks i and j.

In the DDA method used for this article, the Coulomb Mohr criterion and open–close iteration were used to achieve the opening and sliding of the block boundary interface without considering the cracking and failure of the rock block. When two blocks come into contact, the anti-slip force of the block is obtained based on the normal force and friction coefficient and compared with the tangential force. When the tangential force is greater than the anti-slip force, the two blocks slide. In addition, whether the blocks re in contact can be determined based on the distance between them, achieving open–close iteration discrimination.

4. Analysis of Slope Deformation Failure Process

According to geological engineering survey data, the geological cross section shown in Figure 3 was used to represent the quarry slope and simulated by DDA. As the strike of the strata is almost parallel to that of the slope surface, two-dimensional simulation is very suitable for this slope.

Discontinuities were considered in DDA modeling, including fault F12, F17, F18, F90, and F113, as well as the interlayer shear zones buried in different depths. Rock mechanic parameters were derived based upon the rock mechanical test, and they are listed in Table 2. The control parameters used in the calculation of DDA are shown in Table 3. A kinematic damping coefficient of 0.99 was adopted to simulate the energy dissipation during seismic loading in order to account for energy loss mechanisms in DDA. The range of this coefficient is in good agreement with the conclusions of [32]. Additionally, choosing a small allowable maximum step displacement ratio (5×10^{-3} in Table 2) is beneficial in order to promote a precise DDA calculation [31,32,36].

Table 2. Mechanical parameters of the rock strata.

Rock Material	Unit Weight (kN·m ⁻³)	Deformation Modulus (GPa)	Poisson’s Ratio	Cohesion (MPa)	Frictional Coefficient	Tensile Strength (MPa)
Rock strata	26.0	20.0	0.25	1.0	1.0	0.6
Interlayer shear zone	/	/	/	0.05	0.36	0.0
Joint, small fault	23.5	20	0.167	0.1	0.47	0.0

Table 3. Computational control parameters in DDA.

Kinematic Damping Coefficient	Upper Limit of Step Time	Allowable Maximum Step Displacement Ratio	Contact Spring Stiffness
0.99	Automatically selected by the code	5×10^{-3}	30 GN·m ⁻¹

The simulation results show that the slope will fail if excavation is completed without support, and the failure process is shown in Figure 10. Under the effect of gravity, the upper strata of slope initially slip. From the results in Figure 10b, we can find that the middle and upper strata slip along the interlayer shear zones and consequently transmit force to the lower part of strata, causing an active extrusion effect on the lower strata. The lower strata subsequently slip and crack along the joints or small faults and gradually extrude outward, as shown in Figure 10c,d. Finally, in the lower position of the slope, buckling failure occurs, as shown in Figure 10e,f. This is a typical buckling failure mode characterized by upper-slipping followed by lower-buckling. DDA can adequately reveal this mechanism and slope failure process.

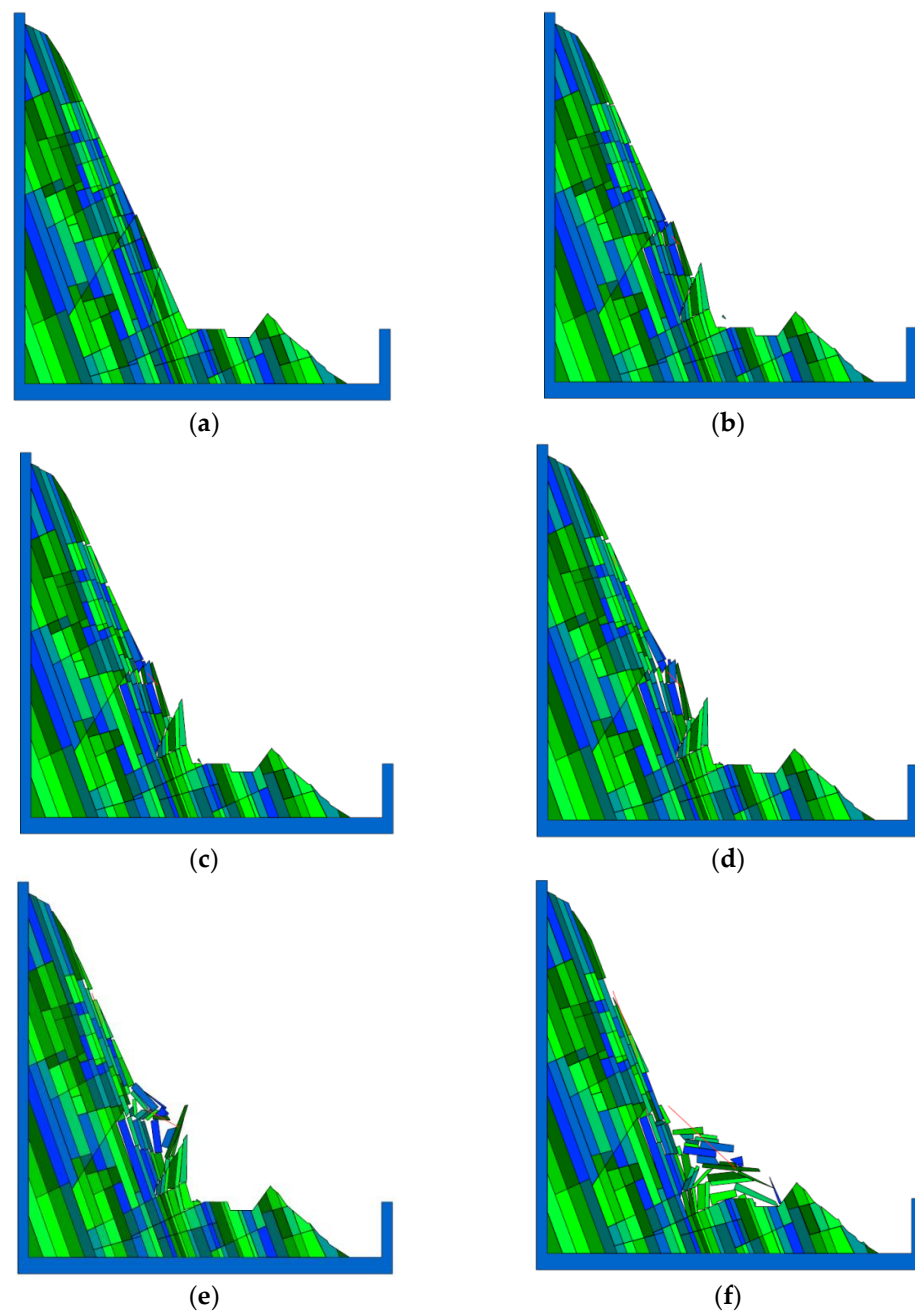


Figure 10. The failure process of the slope simulated via DDA.

The deformation failure mechanism can be attributed to two reasons: one is that the sedimentary rock strata form a mechanical multiple slab structure with densely-developed interlayer shear zones in the strata; the other is that the dip of strata is steep and close to the angle of the excavated slope, forming a favorable condition for slip–buckling deformation.

5. Investigation of Reinforcement Design Scheme

Anchor cables were used to reinforce the slope. The anchor cables we used were 64 m in length and inclined downward 20°. A total of 16 anchor cables were mounted on the 2D section. Compared with the actual spacing of the anchor cables, the ultimate tensile force for each anchor cable was equivalently 1500 t in the 2D section simulation.

After applying the anchor cables, the rock mass of the slope became stable, as shown in Figure 11. The simulated internal force of each anchor cable is shown in Figure 12, where the anchor cables are numbered in sequence from the bottom to the top. The internal forces of the fourth and eighth anchor cables are the largest, and the internal force is larger in the middle and lower parts of the slope, whereas the forces of anchor cables in the upper part of the slope is very small. As a consequence, there is an urgent need to strengthen the support in the middle and lower parts of the slope, and the length and pre-stress of the anchor cables in the upper part of the slope can be properly reduced.

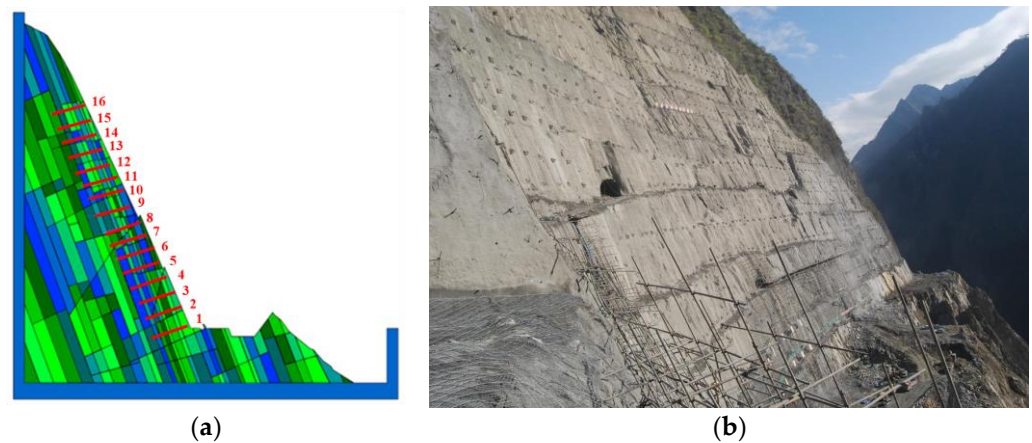


Figure 11. The slope becomes stable after applying anchor cables. (a) Numerical simulation diagram; (b) Live pictures.

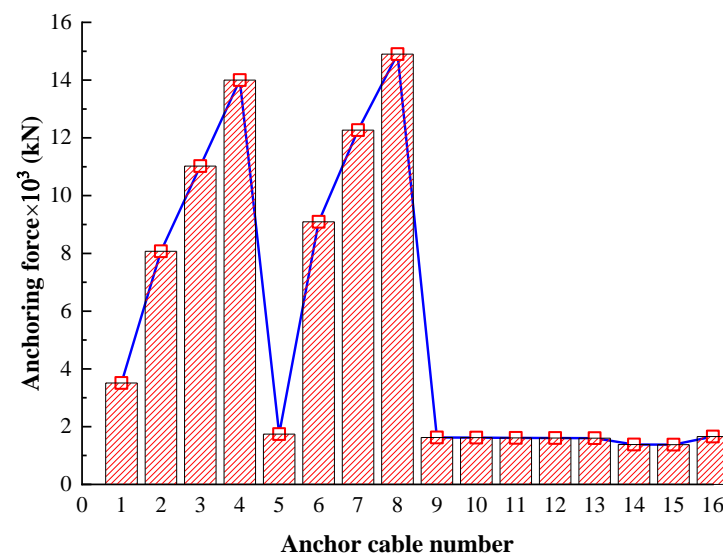


Figure 12. Distribution of anchoring force.

The stability of a slope is not only assessed based on gravity loading but also on earthquake loading. Hence, we further analyzed the stability of the anchored slope considering earthquake action. A real-time seismic recording curve of a magnitude 9.0 earthquake in a certain area was used in our simulation, as shown in Figure 13. By halving or doubling the acceleration factor (the ratio of recorded seismic acceleration to gravity acceleration) in the curve, a magnitude 8.0 or 10.0 earthquake was obtained.

Under a magnitude 8 earthquake, the internal force of the anchor cables in the middle and lower parts exceeds their ultimate tensile force and the anchor cables break down one after another, finally leading to slope failure. This slope failure process is shown in Figure 14.

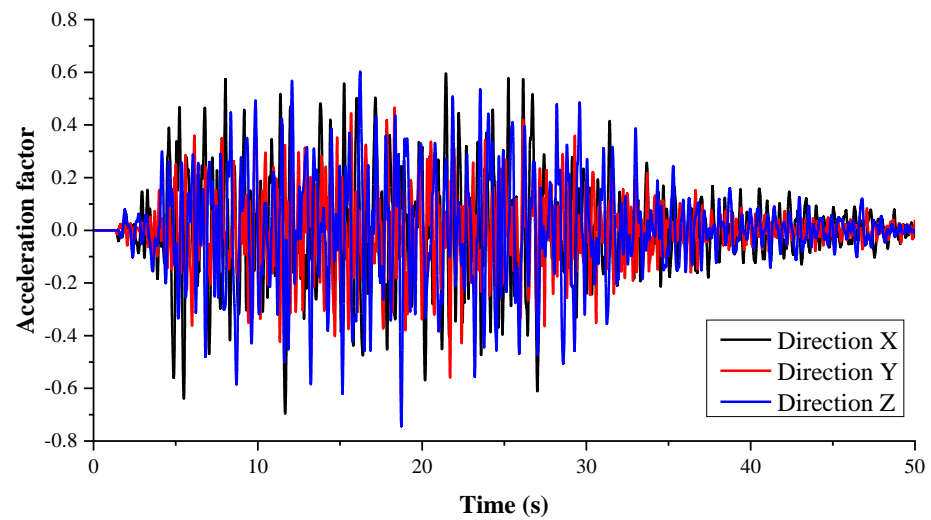


Figure 13. Measured seismic acceleration curve in a certain area.

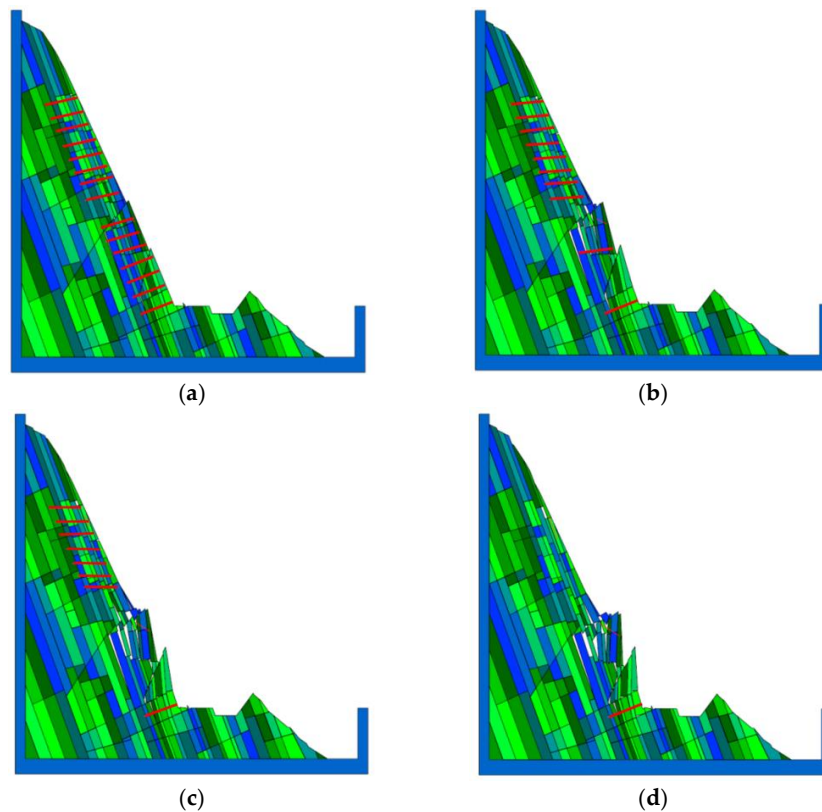


Figure 14. The failure process under a magnitude 8 earthquake.

Based on the above analysis results, the reinforcement scheme was then adjusted: the length of the anchor cables in the upper part of the slope was reduced, the anchoring force was reduced to be 1/3 of the previous designated value, and the quantity of the anchor cable was doubled in the middle and lower parts. Figure 15 shows the final failure state of the slope after the reinforcement scheme was adjusted. Under these conditions, the anchored rock masses are totally stable under a magnitude 7 earthquake, with two anchor cables breaking down in the middle part of the slope. Under a magnitude 8 earthquake, six anchor cables break down one after another when the earthquake lasts for 30 s, and the slope will fail overall; however, there was no evidence of a collapse.

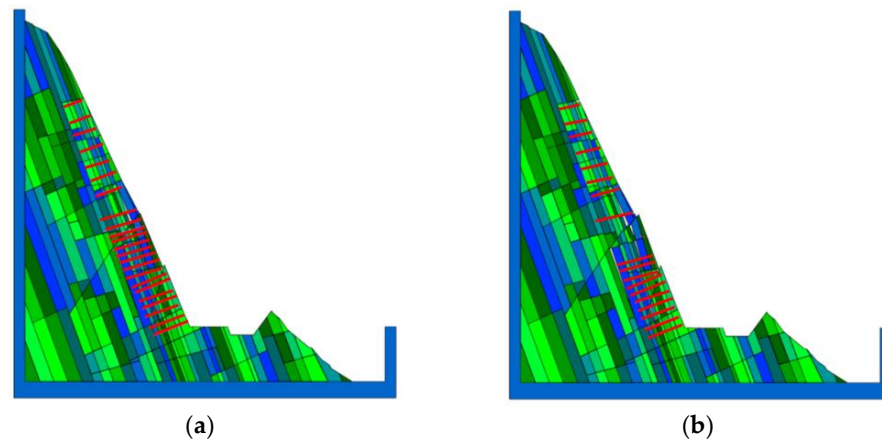


Figure 15. Final failure state of the slope after adjusting the reinforcement scheme. (a) Under a magnitude 7 earthquake. (b) Under a magnitude 8 earthquake.

6. Stability Evaluation of Slope under Reinforcement Scheme

6.1. Monitoring Setting

A monitoring system was designed and installed to examine the stability of the slope during excavation and the performance of reinforcement scheme. It can be divided into three main components: slope surface deformation monitoring, shallow deformation monitoring, and anchoring force monitoring. Through using these measures, we were able to evaluate the deformation of the slope and the anchoring force loss in the anchor cables.

The arrangement of the surface monitoring points aimed to monitor the overall deformation of the slope that was influenced by fault F12, F17, F18, F90, F113, and the interlayer shear zones exposed on the excavation surface. The TCA2003 automatic tracking total station Leica was employed to monitor the surface deformation of the slope. A total of 17 surface observation piers were installed on different levels of the cutting edge of the slope, as denoted from HD1-DBL to HD17-DBL in Figure 16. Amongst these, 6 points were on the excavated slope above 2000 m elevation, and 10 points were located between 1680 and 2000 m.

Multi-point extensometers were employed to monitor the deformation of the rocks that was induced by stress relaxation in the slope at shallow depth (within 40 m beneath the excavated surface). A total of five sets of multi-point extensometers were arranged in the left bank slope, of which one set was located above 2000 m (numbered M1-DBL) and 4 sets were located between 1680 and 2000 m (numbered M2-DBL to M5-DBL). The layout of the multi-point extensometers is plotted in Figure 16.

To monitor the loss of anchoring force, eight cable dynamometers were installed in the pre-stressed anchor cables. Among them, three sets of dynamometers were located above 2000 m, as illustrated in Figure 16. The others were installed below 2000 m elevation.

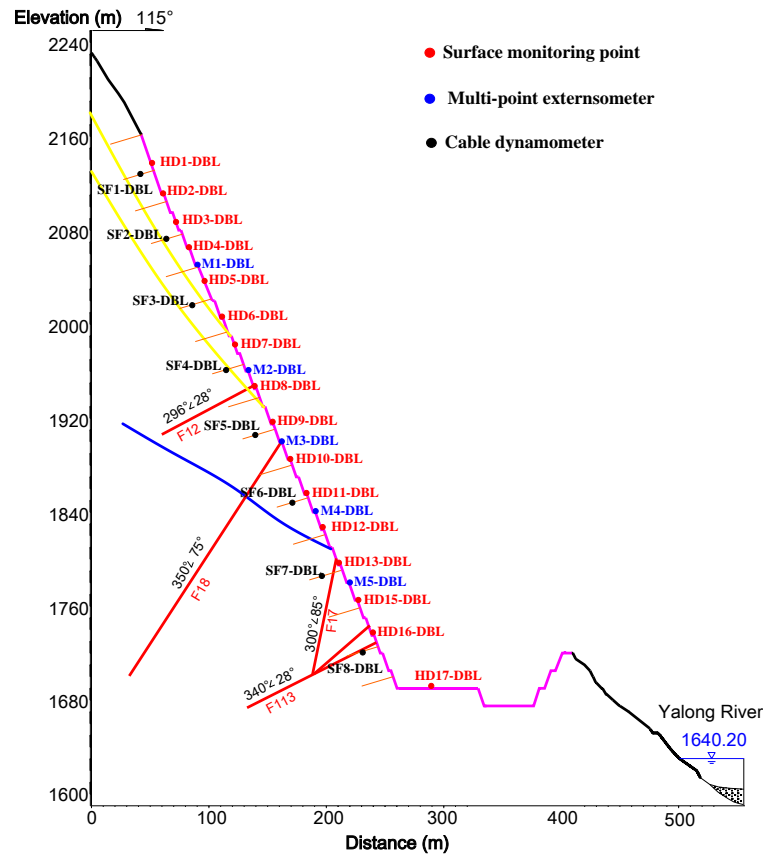


Figure 16. Layout of various monitoring points on the Dabenliu quarry slope.

6.2. Analysis of Monitoring Data

Figure 17 shows the variation in the horizontal deformation of some of the typical surface monitoring points over time. Three slope deformation stages can be observed in Figure 17. In the initial excavation stage, the slope deformed at a low rate because of the small volume of excavation. After 100 days, the slope was excavated rapidly, causing the deformation rate at the surface monitoring points to increase dramatically. When excavation finished, the slope deformation rate slowed down and showed a tendency towards a constant value. A similar deformation trend was also observed for a typical multi-point of M3-DBL, as shown in Figure 18.

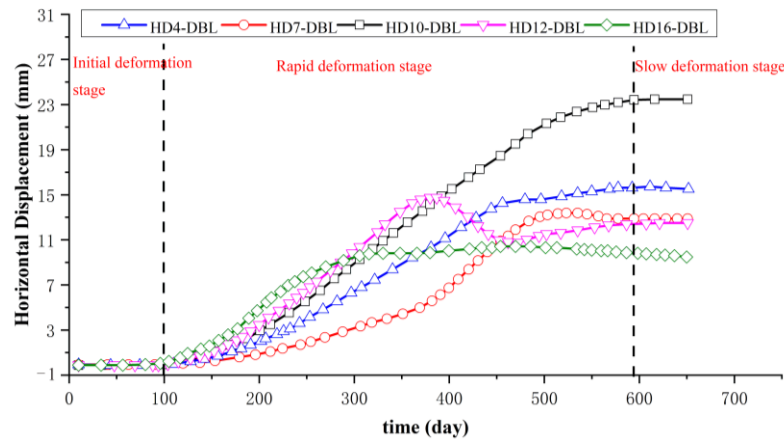


Figure 17. Deformation evolution of typical surface monitoring points (HD4-DBL, HD7-DBL-HD12-DBL, and HD16-DBL) with time.

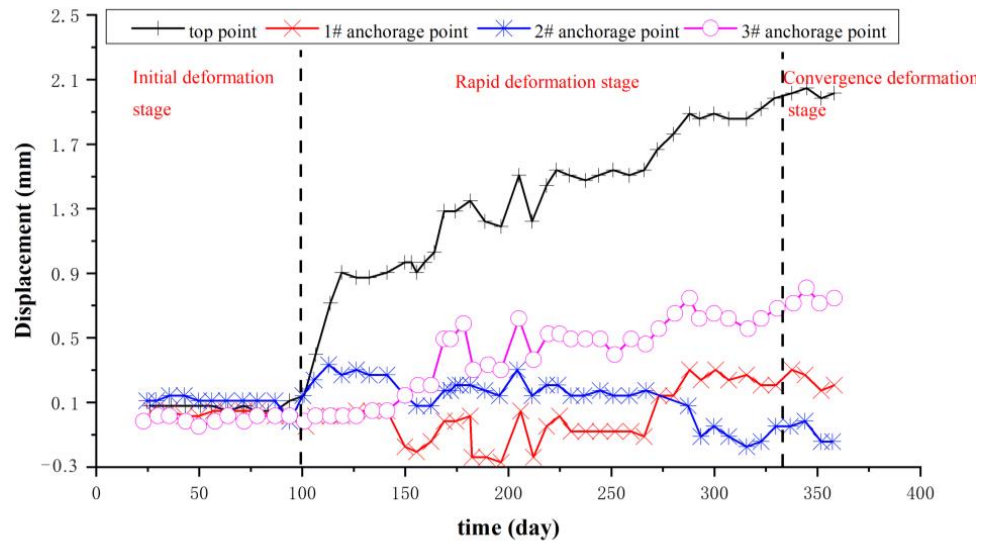


Figure 18. Deformation of evolution of extensometers M2-DBL.

Figure 19 shows the anchoring force and the variation in loss ratio (the ratio of real-time force to the locked force) of SF5_DBL during the excavation process. Initially, the rapid increase in anchoring force is associated with the lack of deep support treatment regarding the excavated slope. When the reinforcement scheme was completed above 1985 m elevation, the anchoring force remained stable. Widespread rainfall in the summer of 2011 led to an obvious increase in anchoring force again. Later, after the completion of excavation and the reinforcement measurements, the anchoring force showed a tendency towards a convergence state, and its anchoring loss ratio was 5.2%, which is acceptable in engineering. Through combining the deformation results of surface deformation monitoring and shallow deformation monitoring, it was shown that the slope is in a stable condition under the implementation of the reinforcement design scheme.

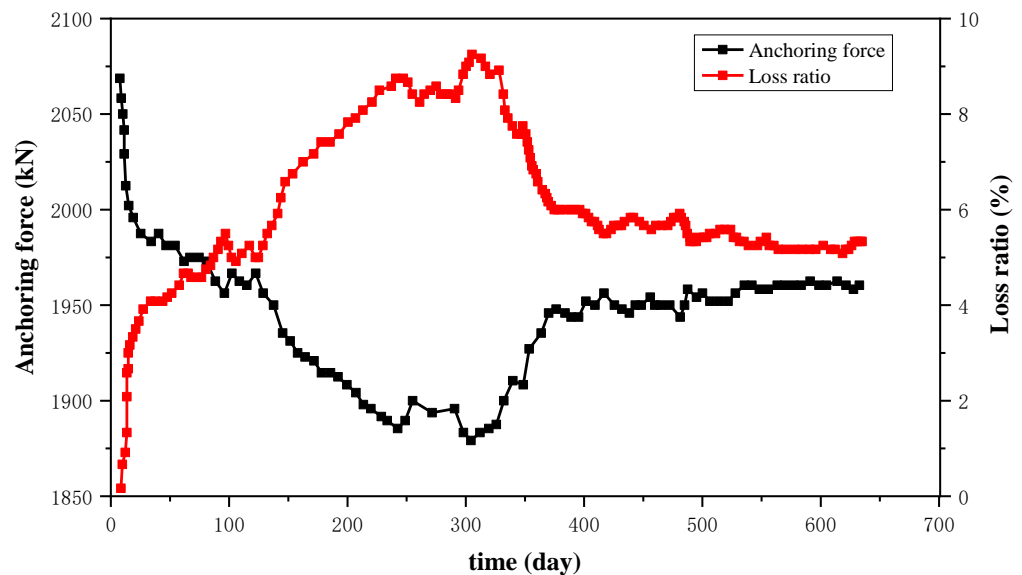


Figure 19. Evolution of anchoring force and loss ratio for dynamometer SF5_DBL.

The DDA simulation results show that the excavated slope is stable under the action of gravity after the reinforcement scheme was implemented. This conclusion is consistent with that of field monitoring studies and the actual behavior of slope. Thus, the use of the DDA method for evaluating the stability of the slope proved to be reasonable.

It should be noted that the monitoring results only reflect the deformation behavior of the slope under gravity loading, and the state of the slope under seismic loading is not known. The DDA method brings the advantage of providing a dynamic solution for discontinuous deformation; therefore, the stability of this slope was extensively evaluated via DDA simulation. The results described in Section 5 also indicate that the slope is stable under the action of a magnitude 7 earthquake.

7. Conclusions

The Dabenliu quarry slope in the Jinping I Hydropower Station is a typical high-steep bedding slope. We initially analyzed the failure modes of the slope. Then, the deformation failure process of the slope after excavation and under earthquake action was simulated using DDA, and the reinforcement design scheme was adjusted accordingly. Finally, our simulation results were verified via a comparison with the monitoring data of the slope. The main conclusions that can be drawn from the present study are as follows:

(1) After the slope is excavated, the middle and upper strata may slip along the interlayers, while the lower part may slip and crack along the joints or small faults and then gradually extrude outward. This is a typical buckling failure mode characterized by upper-slipping followed with lower-buckling. This slope deformation failure process was vividly simulated via DDA simulation. The deformation failure mechanism can be attributed to two reasons: a special mechanical structure in rock strata and an angle relationship favorable for deformation between the strata and the excavated slope.

(2) A method for setting a viscous boundary in the calculation of dynamic deformation under seismic loading and an algorithm for modeling pre-stressed cable were developed. The effect of reinforcing the slope under seismic loading was further discussed. Under the action of a magnitude 8 earthquake, the anchored slope may be instable. Based on the distribution of the simulated internal force of the anchor cables, the reinforcement scheme was adjusted to strengthen the support of the middle and lower parts of the slope and reduce the length and pre-stress of the anchor cables in the upper part. The adjusted reinforcement scheme can maintain the stability of the slope under the action of a magnitude 7 earthquake, but the slope may fail without evident collapse under the action of a magnitude 8 earthquake.

(3) Through a comparison with the monitoring data of the surface, shallow deformation, and anchoring force, it was found that after excavation completion, the deformation of the slope shows a tendency towards a convergence state under the support of the anchor cables, and this is consistent with the results of the DDA simulation. Therefore, the Dabenliu quarry slope is stable and safe. This study also proved that the proposed reinforcement scheme is effective and that the DDA method is a powerful tool for simulating the complex process of rock mass deformation failure under different loading conditions.

Author Contributions: Conceptualization, F.X. and W.-H.H.; methodology, Q.-H.Z.; software, W.-H.H.; validation, W.-H.H., F.X. and Q.-H.Z.; formal analysis, F.X.; investigation, W.-H.H.; resources, F.X.; data curation, Q.-H.Z.; writing—original draft preparation, W.-H.H.; writing—review and editing, F.X.; visualization, W.-H.H.; supervision, W.-H.H.; project administration, Q.-H.Z.; funding acquisition, F.X. All authors have read and agreed to the published version of the manuscript.

Funding: This research was funded by the General Program of the National Natural Science Foundation of China (Grant number 52079129, 52209148).

Institutional Review Board Statement: Not applicable.

Informed Consent Statement: Not applicable.

Data Availability Statement: Not applicable.

Conflicts of Interest: The authors declare no conflict of interest.

References

1. Tang, S.B.; Huang, R.Q.; Wang, S.Y.; Bao, C.Y.; Tang, C.A. Study of the fracture process in heterogeneous materials around boreholes filled with expansion cement. *Int. J. Solids Struct.* **2017**, *112*, 1–15. [[CrossRef](#)]
2. Tang, S.; Wang, J.; Chen, P. Theoretical and numerical studies of cryogenic fracturing induced by thermal shock for reservoir stimulation. *Int. J. Rock Mech. Min. Sci.* **2020**, *125*, 104160. [[CrossRef](#)]
3. Tang, S.B.; Zhang, H.; Tang, C.A.; Liu, H.Y. Numerical model for the cracking behavior of heterogeneous brittle solids subjected to thermal shock. *Int. J. Solids Struct.* **2016**, *80*, 520–531. [[CrossRef](#)]
4. Tang, S.B.; Tang, C.A. Crack propagation and coalescence in quasi-brittle materials at high temperatures. *Eng. Fract. Mech.* **2015**, *134*, 404–432. [[CrossRef](#)]
5. Tang, S.B.; Tang, C.A.; Zhu, W.C.; Wang, S.H.; Yu, Q.L. Numerical investigation on rock failure process induced by thermal stress. *Chin. J. Rock Mech. Eng.* **2006**, *25*, 2071–2078. (In Chinese)
6. Qin, S.; Jiao, J.J.; Wang, S. A cusp catastrophe model of instability of slip-buckling slope. *Rock Mech. Rock Eng.* **2001**, *34*, 119–134. [[CrossRef](#)]
7. MacLaughlin, M.M.; Doolin, D.M. Review of validation of the discontinuous deformation analysis (DDA) method. *Int. J. Numer. Anal. Methods Geomech.* **2006**, *30*, 271–305. [[CrossRef](#)]
8. Feng, X.; Jiang, Q.; Zhang, X.; Zhang, H. Shaking table model test on the dynamic response of anti-dip rock slope. *Geotech. Geol. Eng.* **2019**, *37*, 1211–1221. [[CrossRef](#)]
9. Bao, H.; Zhao, Z.; Tian, Q. On the Implementation of augmented Lagrangian method in the two-dimensional discontinuous deformation Analysis. *Int. J. Numer. Anal. Methods Geomech.* **2014**, *38*, 551–571. [[CrossRef](#)]
10. Wu, W.; Wang, X.; Zhu, H.; Shou, K.-J.; Lin, J.-S.; Zhang, H. Improvements in DDA program for rockslides with local in-circle contact method and modified open-close iteration. *Eng. Geol.* **2020**, *265*, 105433. [[CrossRef](#)]
11. Yeung, M.; Jiang, Q.; Sun, N. Validation of block theory and three-dimensional discontinuous deformation analysis as wedge stability analysis methods. *Int. J. Rock Mech. Min. Sci.* **2003**, *40*, 265–275. [[CrossRef](#)]
12. Ma, G.; Matsuyama, H.; Nishiyama, S.; Ohnishi, Y. Practical studies on rockfall simulation by DDA. *J. Rock Mech. Geotech. Eng.* **2011**, *3*, 57–63. [[CrossRef](#)]
13. Zhang, Q.-H.; Shi, G.-H. Verification of a DDA-based hydro-mechanical model and its application to dam foundation stability analysis. *Int. J. Rock Mech. Min. Sci.* **2021**, *138*, 104627. [[CrossRef](#)]
14. Yin, Q.; Liu, R.; Jing, H.; Su, H.; Yu, L.; He, L. Experimental study of nonlinear flow behaviors through fractured rock samples after high-temperature exposure. *Rock Mech. Rock Eng.* **2019**, *52*, 2963–2983. [[CrossRef](#)]
15. Yin, Q.; Wu, J.Y.; Zhu, C.; He, M.C.; Meng, Q.X.; Jing, H.W. Shear mechanical responses of sandstone exposed to high temperature under constant normal stiffness boundary conditions. *Geomech. Geophys. Geo-Energy Geo-Resour.* **2021**, *7*, 35. [[CrossRef](#)]
16. Yin, Q.; Wu, J.; Zhu, C.; Wang, Q.; Zhang, Q.; Jing, H.; Xie, J.Y. The role of multiple heating and water cooling cycles on physical and mechanical responses of granite rocks. *Geomech. Geophys. Geo-Energy Geo-Resour.* **2021**, *7*, 69. [[CrossRef](#)]
17. Xiong, F.; Zhu, C.; Feng, G.; Zheng, J.; Sun, H. A three-dimensional coupled thermo-hydro model for geothermal development in discrete fracture networks of hot dry rock reservoirs. *Gondwana Res.* **2023**, *122*, 331–347. [[CrossRef](#)]
18. Tommasi, P.; Verrucci, L.; Campedel, P.; Veronese, L.; Pettinelli, E.; Ribacchi, R. Buckling of high natural slopes: The case of Lavini di Marco (Trento-Italy). *Eng. Geol.* **2009**, *109*, 93–108. [[CrossRef](#)]
19. Seijmonsbergen, A.; Woning, M.; Verhoef, P.; Graaff, L. The failure mechanism of a late glacial sturzstrom in the Subalpine Molasse (Leckner Valley, Vorarlberg, Austria). *Geomorphology* **2005**, *66*, 277–286. [[CrossRef](#)]
20. Tang, S.; Huang, R.; Tang, C.; Liang, Z.; Heap, M. The failure processes analysis of rock slope using numerical modelling techniques. *Eng. Fail. Anal.* **2017**, *79*, 999–1016. [[CrossRef](#)]
21. Wang, W.; Chen, G.; Zhang, Y.; Zheng, L.; Zhang, H. Dynamic simulation of landslide dam behavior considering kinematic characteristics using a coupled DDA-SPH method. *Eng. Anal. Bound. Elem.* **2017**, *80*, 172–183. [[CrossRef](#)]
22. Shi, G. Discontinuous Deformation Analysis: A New Numerical Model for the Statics and Dynamics of Block Systems. Ph.D. Dissertation, University of California, Berkeley, CA, USA, 1988.
23. Shi, G. Rock stability analysis and three convergences of discontinuous deformation analysis (DDA). In Proceedings of the 9th International Conference on Analysis of Discontinuous Deformation: New Development and Applications, Singapore, 27–29 November 2009; pp. 1–11.
24. Hatzor, Y.; Feintuch, A. The validity of dynamic block displacement prediction using DDA. *Int. J. Rock Mech. Min. Sci.* **2001**, *38*, 599–606. [[CrossRef](#)]
25. Tsesarsky, M.; Hatzor, Y.; Sitar, N. Dynamic block displacement prediction—validation of DDA using analytical solutions and shaking table experiments. In *Stability of Rock Structures, Proceedings of the Fifth International Conference of Analysis of Discontinuous Deformation, Beer Sheva, Israel, 6–10 October 2002*; Hatzor, Y.H., Ed.; Balkema: Lisse, The Netherlands, 2002; pp. 195–203.
26. Doolin, D.; Sitar, N. Displacement accuracy of discontinuous deformation analysis method applied to sliding block. *J. Eng. Mech.* **2002**, *128*, 1158–1168. [[CrossRef](#)]
27. Irie, K.; Koyama, T.; Nishiyama, S.; Yasuda, Y.; Ohnishi, Y. A numerical study on the effect of shear resistance on the landslide by Discontinuous Deformation Analysis (DDA). *Geomech. Geoengin.* **2012**, *7*, 57–68. [[CrossRef](#)]
28. Shi, G. Contact theory. *Sci. China Technol. Sci.* **2015**, *58*, 1–47. [[CrossRef](#)]

29. Jiang, Q.-H.; Yeung, M.R. A model of point-to-face contact for three-dimensional discontinuous deformation analysis. *Rock. Mech. Rock. Eng.* **2004**, *37*, 95–116. [[CrossRef](#)]
30. Grayeli, R.; Hatami, K. Implementation of the finite element method in the three-dimensional discontinuous deformation analysis (3D-DDA). *Int. J. Numer. Anal. Methods Geomech.* **2008**, *32*, 1883–1902. [[CrossRef](#)]
31. Ma, K.; Liu, G.; Guo, L.; Zhuang, D.; Collins, D. Deformation and stability of a discontinuity-controlled rock slope at Dagangshan hydropower station using three-dimensional discontinuous deformation analysis. *Int. J. Rock Mech. Min. Sci.* **2020**, *130*, 104313. [[CrossRef](#)]
32. Hatzor, Y.; Arzi, A.; Zaslavsky, Y.; Shapira, A. Dynamic stability analysis of jointed rock slopes using the DDA method: King Herod's Palace, Masada, Israel. *Int. J. Rock Mech. Min. Sci.* **2004**, *41*, 813–832. [[CrossRef](#)]
33. Wu, J.-H.; Lin, J.-S.; Chen, C.-S. Dynamic discrete analysis of an earthquake-induced large-scale landslide. *Int. J. Rock Mech. Min. Sci.* **2009**, *46*, 397–407. [[CrossRef](#)]
34. Wu, J.-H. Seismic landslide simulations in discontinuous deformation analysis. *Comput. Geotech.* **2010**, *37*, 594–601. [[CrossRef](#)]
35. Zhang, Y.; Wang, J.; Xu, Q.; Chen, G.; Zhao, J.X.; Zheng, L.; Han, Z.; Yu, P. DDA validation of the mobility of earthquake-induced landslides. *Eng. Geol.* **2015**, *194*, 38–51. [[CrossRef](#)]
36. Gong, S.; Hu, C.; Guo, L.; Ling, D.; Chen, G.; Zhang, X. Extended DDA with rotation remedies and cohesive crack model for simulation of the dynamic seismic landslide. *Eng. Fract. Mech.* **2022**, *266*, 108395. [[CrossRef](#)]
37. Shi, G. Applications of discontinuous deformation analysis (DDA) to rock stability analysis. In Proceedings of the 8th International Conference on Analysis of Discontinuous Deformation: Fundamentals and Applications to Mining and Civil Engineering, Beijing, China, 14–19 August 2007; pp. 1–14.
38. Tsesarsky, M.; Hatzor, Y.H. Tunnel roof deflection in blocky rock masses as a function of joint spacing and friction—A parametric study using discontinuous deformation analysis (DDA). *Tunn. Undergr. Space Technol.* **2006**, *21*, 29–45. [[CrossRef](#)]
39. Ohnishi, Y.; Nishiyama, S. Recent insights of analyses using discontinuous methods in rock engineering in Japan. In Proceedings of the 8th International Conference on Analysis of Discontinuous Deformation: Fundamentals and Applications to Mining and Civil Engineering, Beijing, China, 14–19 August 2007; pp. 15–26.
40. Huang, D.; Li, Y.Q.; Song, Y.X.; Xu, Q.; Pei, X.J. Insights into the catastrophic Xinmo rock avalanche in Maoxian county, China: Combined effects of historical earthquakes and landslide amplification. *Eng. Geol.* **2019**, *258*, 105158. [[CrossRef](#)]

Disclaimer/Publisher's Note: The statements, opinions and data contained in all publications are solely those of the individual author(s) and contributor(s) and not of MDPI and/or the editor(s). MDPI and/or the editor(s) disclaim responsibility for any injury to people or property resulting from any ideas, methods, instructions or products referred to in the content.